RESEARCH ARTICLE | NOVEMBER 01 1985

Kinetic theory of stimulated Raman sidescattering from magnetized plasmas

R. Rankin; T. J. M. Boyd

Phys. Fluids 28, 3380–3386 (1985)
https://doi.org/10.1063/1.865337

Kinetic theory of stimulated Raman sidescattering from magnetized plasmas

R. Rankin[a] and T. J. M. Boyd
Department of Physics, University College of North Wales, Bangor, Gwynedd LL57 2UW, Wales

(Received 10 October 1984; accepted 1 May 1985)

A theory of stimulated Raman sidescattering in magnetized plasmas is presented based on a solution of the Vlasov–Maxwell equations. The incident laser light, in the form of extraordinary mode radiation, decays into light waves which propagate along the uniform magnetic field as right or left circularly polarized waves. The scattered plasma mode is an obliquely propagating electron-Bernstein wave. The possible relevance of the theory to experiments in which structure is observed in radiation at one-half of the laser frequency is discussed.

I. INTRODUCTION

Stimulated Raman scattering (SRS)[1–4] in laser target plasmas can have potentially serious consequences as far as the efficient coupling of radiation to laser produced plasmas is concerned. This instability—a three-wave parametric process in which the incident laser light decays into an electron plasma wave and a scattered light wave—generates very high energy electrons[5–8] which can preheat the interior of fusion targets. In addition, for reactor size targets a sizeable fraction of the incident laser light may be scattered out of the plasma by this process. Both of these effects run counter to the aims of effective inertial confinement.

The recent resurgence of interest in stimulated Raman scattering has been caused in no small measure by the switch away from short-pulse high irradiance experiments ($I_L \sim 10^{15}$–10^{16} W cm^{-2} with τ_L in tens of picoseconds, where I_L represents the laser intensity and τ_L the pulse length) to the present preoccupation with long scale length plasmas[9–14] generated by relatively modest intensity laser pulses ($I_L \lesssim 10^{14}$ W cm^{-2}) of long duration (of the order of nanoseconds). Plasmas generated in this way can extend over hundreds of laser wavelengths and can result in SRS reflectivities of several percent.[8] Also, when the plasma is of sufficient extent laterally, stimulated Raman sidescattering (SRSS) occurs at a lower threshold intensity than backscatter. This has potentially serious consequences in large volume plasmas since the convective growth of the instability is not limited by Landau damping of plasma waves (as occurs in the case of backscatter) so that a substantial amplification may result.

In previously published work[15] we drew attention to the importance of magnetic fields on stimulated Raman scattering. In particular, it was shown that for backscatter the field enhanced the instability and if sufficiently large enough could change the usual red shift in the $\omega_0/2$ scattered light wave (ω_0 is the laser frequency) to a blue shift. Using a fluid model of the plasma we also studied the effects of magnetic fields on Raman sidescatter. The decay examined was one where the sidescattered light waves propagated along the magnetic field lines as right and left circularly polarized light waves. The motivation for this study was prompted by experiments[10–13] in which the Raman light exhibited a doublet structure with red and blue wings with respect to the frequency $\omega_0/2$. It is obvious that when sufficiently large magnetic fields (on the megagauss scale) exist in the plasma, double-peaked emission becomes possible if right and left circularly polarized waves can be driven unstable. To account for observations at laser wavelengths less than or equal to one micron, this model requires fields approximately twice the magnitude (i.e., 7 MG) of any thus far reported. However, it is important to make an estimate of the splitting which could be induced by magnetic fields alone.

There is now widespread evidence[16–20] for megagauss fields in certain laser-generated plasmas. Work by Raven *et al.*,[18] for example, showed that fields can be large in the neighborhood of the quarter-critical density of the plasma, where the Raman decay takes place. Max[21] has earlier drawn attention to the variety of mechanisms in addition to the $\nabla N \times \nabla T$ source by which large magnetic fields may be generated. Possible sources include filamentation of the laser light[22]; this process has a high gain in long scale length plasmas. Other sources that may give rise to small scale fields are Weibel-type instabilities[23]; there is some evidence for micromagnetic fields of up to 5 MG in laser-produced plasmas.[24]

In our previous treatment of stimulated Raman sidescattering[15] we neglected finite Larmor radius effects; this assumption is not generally valid with megagauss fields present, since then $kr_L \sim 1$, where k is the wavenumber of electron plasma waves and r_L is the electron Larmor radius. In this paper we present a full kinetic treatment of the decay of extraordinary mode laser light (with wavenumber $\mathbf{k}_0$, wave magnetic field $\mathbf{B}_0$ such that $\mathbf{k}_0 \perp \mathbf{B}_c \| \mathbf{B}_0$, where $\mathbf{B}_c$ represents a dc magnetic field) into scattered right and left circularly polarized electromagnetic waves together with electron-Bernstein waves directed obliquely to the magnetic field. The coupled-mode equations for this process are developed in Sec. II. In Sec. III we describe results from a numerical solution of the equations, and in Sec. IV our conclusions are stated.

II. COUPLED MODE EQUATIONS FOR RAMAN SIDESCATTER

The coupled mode equations needed for a description of Raman sidescattering are found from the set of Vlasov–Maxwell equations

$$\frac{\partial f}{\partial t} + \mathbf{v}\cdot\nabla f - \frac{e}{m}\left(\mathbf{E} + \frac{\mathbf{v}\times\mathbf{B}}{c}\right)\cdot\nabla_{\mathbf{v}} f = 0, \tag{1}$$

$$\nabla\cdot\mathbf{E} = -4\pi ne\int f\,d\mathbf{v}, \tag{2}$$

$$\nabla\times\mathbf{E} = -\frac{1}{c}\frac{\partial\mathbf{B}}{\partial t}, \tag{3}$$

[a] Present address: Department of Electrical Engineering, The University of Alberta, Edmonton, Alberta, Canada T6G 2E1.

 0031-9171/85/113380-07$01.90

$$\nabla\times\mathbf{B}=\frac{1}{c}\frac{\partial\mathbf{E}}{\partial t}+\frac{4\pi}{c}\mathbf{J}. \tag{4}$$

In (1)–(4), $\mathbf{E}$ represents the electric field, $\mathbf{B}$ is the magnetic field, e is the electron charge, m is its mass, n is the average electron number density, $\mathbf{J}$ is the current density, f is the electron distribution function, and c is the speed of light; ion motion is neglected.

The laser light (incident in the x direction) is in the form of an extraordinary mode with electric field components E_{0x} and E_{0y}. As usual, for densities much less than the critical density n_c and magnetic field strengths such that the electron-cyclotron frequency is much less than ω_0, we may ignore E_{0x} compared to E_{0y}; thus $\mathbf{E}_0=\frac{1}{2}E_{0y}\hat{\mathbf{y}}\exp[i(\mathbf{k}_0\cdot\mathbf{x}-\omega_0 t)]+$ complex conjugate. We consider the decay of the incident light into right and left circularly polarized electromagnetic waves together with obliquely propagating electron Bernstein waves. Thus the scattered light waves have both perpendicular, $k_\perp$, and parallel, $k_\parallel$, wavenumber components. Furthermore, for simplicity we shall make an electrostatic approximation in describing the Bernstein waves. As discussed elsewhere,[15] the effects we wish to describe are not seriously affected by making use of these approximations.

The system is perturbed from its equilibrium state according to

$$f=f_0^0+f_0+f_1,$$
$$\mathbf{E}=\mathbf{O}+\mathbf{E}_0+\mathbf{E}_1,$$
$$\mathbf{B}=\mathbf{B}_c+\mathbf{B}_0+\mathbf{B}_1,$$

where f_0^0 represents the unperturbed electron distribution function (taken to be Maxwellian), f_0 represents the contribution from the laser light, and f_1 is produced as a result of the coupling between the normal modes of the system. The laser light electric (magnetic) field $\mathbf{E}_0(\mathbf{B}_0)$ gives rise to perturbed fields $\mathbf{E}_1(\mathbf{B}_1)$, and $\mathbf{B}_c$ represents the static magnetic field. On substituting this set of variables into the Vlasov equation we obtain an equation relating f_1 to $\mathbf{E}_0$, namely,

$$\frac{\partial f_1}{\partial t}+\mathbf{v}\cdot\nabla f_1+(\mathbf{v}\times\boldsymbol{\Omega})\cdot\nabla_{\mathbf{v}}f_1$$
$$=\frac{e}{m}\left(\mathbf{E}_1+\frac{\mathbf{v}\times\mathbf{B}_1}{c}\right)\cdot\nabla_{\mathbf{v}}f_0^0$$
$$+\frac{e}{m}\left(\mathbf{E}_0+\frac{\mathbf{v}\times\mathbf{B}_0}{c}\right)\cdot\nabla_{\mathbf{v}}f_1 \tag{5}$$

in which $\boldsymbol{\Omega}=-eB_c/m\hat{\mathbf{z}}$ is the electron-cyclotron frequency.

The Vlasov equation is solved by integrating along the unperturbed electron trajectories and to do this it is first convenient to isolate that part of Eq. (5) which describes coupling of the different waves to $\mathbf{E}_0$. Thus we express f_1 as $f_1^L+f_1^{NL}$ and consider the following two equations:

$$Lf_1^L=\frac{e}{m}\left(\mathbf{E}_1+\frac{\mathbf{v}\times\mathbf{B}_1}{c}\right)\cdot\nabla_{\mathbf{v}}f_0^0, \tag{6a}$$

$$Lf_1^{NL}=\frac{e}{m}\left(\mathbf{E}_1+\frac{\mathbf{v}\times\mathbf{B}_1}{c}\right)\cdot\nabla_{\mathbf{v}}f_0$$
$$+\frac{e}{m}\left(\mathbf{E}_0+\frac{\mathbf{v}\times\mathbf{B}_0}{c}\right)\cdot\nabla_{\mathbf{v}}f_1^L, \tag{6b}$$

in which L represents the Vlasov propagator $\partial/\partial t+\mathbf{v}\cdot\nabla+(\mathbf{v}\times\boldsymbol{\Omega})\cdot\nabla_{\mathbf{v}}$. The first equation simply leads to the linear dispersion relation of each wave, whereas the second describes coupling between the different normal modes. The linear dispersion relations are obtained on using (1)–(4) with f_1^L determined according to

$$f_1^L=-\frac{e}{m}\int_{-\infty}^{0}\hat{\mathbf{E}}\cdot\nabla_{\mathbf{v}}f_0^0e^{-i(\mathbf{k}_1\cdot\mathbf{X}-\omega_1\tau)}d\tau, \tag{7}$$

in which $\mathbf{X}=\mathbf{x}-\mathbf{x}'$, $\tau=t-t'$, and $\omega_1(k_1)$ is the frequency (wavenumber) of the particular mode (extraordinary, right or left circularly polarized or electron-Bernstein waves) under investigation. The hat over a quantity indicates the absence of $\exp i(\mathbf{k}_1\cdot\mathbf{x}-\omega_1 t)$. In what follows, the three-wave interaction describing SRSS is assumed to satisfy phase-matching conditions of the form $\omega_-=\omega-\omega_0$, $\mathbf{k}_-=\mathbf{k}-\mathbf{k}_0$. The notation is chosen such that $\mathbf{E}_-(\omega_-,\mathbf{k}_-)$ represents the electric field of the scattered light waves, $\mathbf{E}(\omega,\mathbf{k})$ that of the Bernstein waves, and $\mathbf{E}_0(\omega_0,\mathbf{k}_0)$ that of the pump. For future reference, the various linear distribution functions are as follows:

(i) Extraordinary waves, $k_\parallel=0$,

$$f_0=-\frac{eE_{0y}}{m}\frac{\partial f_0^0}{\partial v_\perp}\exp\left(i\frac{k_0v_\perp}{\Omega}\sin\theta\right)$$
$$\times\sum_{n=-\infty}^{+\infty}\frac{J_n'e^{-in\theta}}{\omega_0-n\Omega}. \tag{8}$$

(ii) Right and left circularly polarized waves, $k_\perp=0$,

$$f_R^L=\frac{ieE_R}{2m}\frac{\partial f_0^0/\partial v_\perp e^{-i\theta}}{\omega_--\Omega-k_\parallel v_\parallel}, \tag{9}$$

$$f_L^L=\frac{ieE_L}{2m}\frac{\partial f_0^0/\partial v_\perp e^{+i\theta}}{\omega_-+\Omega-k_\parallel v_\parallel}, \tag{10}$$

where $E_R=E_{x_-}+iE_{y_-}$ and $E_L=E_{x_-}-iE_{y_-}$.

(iii) Electron-Bernstein waves $k_\perp=k_0$,

$$f_\phi=\frac{2e\phi}{m}\frac{\partial f_0^0}{\partial v_\perp^2}\exp\left(i\frac{k_0v_\perp}{\Omega}\sin\theta\right)$$
$$\times\sum_{n=-\infty}^{+\infty}\left(\frac{\omega}{\omega-n\Omega-k_\parallel v_\parallel}-1\right)J_ne^{-in\theta}, \tag{11}$$

where $\phi(\omega,\mathbf{k})$ is the electrostatic potential of the Bernstein waves.

In these expressions, $v_\perp$, $v_\parallel$ are the usual velocity components perpendicular and parallel to the magnetic field; the argument of the Bessel functions is $k_0v_\perp/\Omega$. The nonlinear dispersion relation to be found can be constructed symbolically as follows. Since the Bernstein waves are coupled to both right and left circularly polarized waves, the dispersion relation which conventionally describes them will be modified so that we can write (with $v_0=eE_{0y}/m\omega_0$)

$$\epsilon\phi=(C_RE_R+C_LE_L)v_0. \tag{12}$$

Here ϵ is the linear dispersion relation describing obliquely propagating Bernstein waves and $C_{R,L}$ represent coupling coefficients. Likewise E_R and E_L are both coupled to ϕ so that

$$\epsilon_RE_R=B_R\phi v_0^*,$$

$$\epsilon_L E_L = B_L \phi v_0^*, \tag{13}$$

where $\epsilon_{R,L}$ is the dispersion relation corresponding to $\mathbf{E}_{R,L}$, respectively. On eliminating E_R and E_L from (13) and substituting into (12), we obtain the nonlinear dispersion relation describing the instability in the form

$$\epsilon = \left(\frac{B_R C_R}{\epsilon_R} + \frac{B_L C_L}{\epsilon_L}\right)|v_0|^2. \tag{14}$$

Thus, the problem is reduced to finding expressions for B and C. Consider first of all the electrostatic waves described by Poissons equation [Eq. (1) with $\mathbf{E} = -i\mathbf{k}\phi$] which will be written in the form

$$k^2\phi = -4\pi ne\int f_\phi \, d\mathbf{v}. \tag{15}$$

Setting $f_\phi = f_\phi^L + f_\phi^{NL}$ as before (15) becomes

$$k^2\phi + 4\pi ne\int f_\phi^L \, d\mathbf{v} = -4\pi ne\int f_\phi^{NL} \, d\mathbf{v}.$$

With f_ϕ defined by (11) we can rewrite this equation in the form

$$\epsilon\phi = -4\pi ne\int f_\phi^{NL} \, d\mathbf{v}, \tag{16}$$

with ϵ given by

$$\epsilon = k^2 + \frac{\omega_p^2}{V_e^2}\sum_{n=-\infty}^{+\infty} I_n(\beta)e^{-\beta} \times\left[1 + \frac{\omega}{\sqrt{2}k_\parallel V_e} Z\left(\frac{\omega - n\Omega}{\sqrt{2}k_\parallel V_e}\right)\right]. \tag{17}$$

In this expression ω_p is the plasma frequency, V_e is the electron thermal velocity, I_n is a modified Bessel function of the first kind, $\beta = k_0^2 V_e^2/\Omega^2$, and Z is the plasma dispersion (Fried–Conte) function. The nonlinear contribution to f_ϕ is determined from Eq. (6b), i.e.,

$$\hat{f}_\phi^{NL}(\mathbf{v}) = -\frac{e}{2m}\int_{-\infty}^{0} d\tau \exp -i(\mathbf{k}\cdot\mathbf{X} - \omega\tau) \times\left\{\frac{\partial \hat{f}_-^{L'}}{\partial \mathbf{v}'}\cdot\left[\left(1 - \frac{\mathbf{k}_0\cdot\mathbf{v}'}{\omega_0}\right)\mathbf{I} + \frac{\mathbf{k}_0\mathbf{v}'}{\omega_0}\right]\cdot\hat{\mathbf{E}}_0 + \frac{\partial \hat{f}_0'}{\partial \mathbf{v}'}\cdot\left[\left(1 - \frac{\mathbf{k}_-\cdot\mathbf{v}'}{\omega_-}\right)\mathbf{I} + \frac{\mathbf{k}_-\mathbf{v}'}{\omega_0}\right]\cdot\hat{\mathbf{E}}_-\right\}, \tag{18}$$

where $f_-^L = f_R^L + f_L^L$ and $\mathbf{k} = k_0\hat{\mathbf{x}} + k_\parallel\hat{\mathbf{z}}$.

The dispersion relations for the scattered electromagnetic waves can be put in the form (13) on using (1)–(4) to construct the quantity

$$\left(\frac{\omega_-^2}{c^2} - k_\parallel^2\right)(E_{x-} \pm iE_{y-}) - i\frac{\omega_-}{c^2}4\pi ne\int (v_x \pm iv_y)f_-^L \, d\mathbf{v} = i\frac{\omega_-}{c^2}4\pi ne\int (v_x \pm iv_y)f_-^{NL} \, d\mathbf{v}. \tag{19}$$

With f_-^L defined by Eqs. (9) and (10), the right-hand side of the above equation gives the terms ϵ_R and ϵ_L so that we may write

$$\epsilon_R E_R = i\frac{\omega_-}{c^2}4\pi ne\int (v_x + iv_y)f_-^{NL} \, d\mathbf{v}, \tag{20}$$

$$\epsilon_L E_L = i\frac{\omega_-}{c^2}4\pi ne\int (v_x - iv_y)f_-^{NL} \, d\mathbf{v}, \tag{21}$$

which is the required form (13). Standard expressions for ϵ_R and ϵ_L are defined below:

$$\epsilon_R = \frac{\omega_-^2}{c^2} - k_\parallel^2 + \frac{\omega_-\omega_p^2}{\sqrt{2}k_\parallel V_e c^2} Z\left(\frac{\omega_- - \Omega}{\sqrt{2}k_\parallel V_e}\right), \tag{22}$$

$$\epsilon_L = \frac{\omega_-^2}{c^2} - k_\parallel^2 + \frac{\omega_-\omega_p^2}{\sqrt{2}k_\parallel V_e c^2} Z\left(\frac{\omega_- + \Omega}{\sqrt{2}k_\parallel V_e}\right). \tag{23}$$

Again we use Eq. (6b) to determine the nonlinear contribution to f_-:

$$\hat{f}_-^{NL}(\mathbf{v}) = -\frac{e}{2m}\int_{-\infty}^{0} d\tau \exp -i(\mathbf{k}_-\cdot\mathbf{x} - \omega_-\tau) \times\left\{\frac{\partial \hat{f}^{L'}}{\partial \mathbf{v}'}\cdot\left[\left(1 - \frac{\mathbf{k}_0\cdot\mathbf{v}'}{\omega_0}\right)\mathbf{I} + \frac{\mathbf{k}_0\mathbf{v}'}{\omega_0}\right]\cdot\hat{\mathbf{E}}_0^* + \frac{\partial \hat{f}_0^{*\prime}}{\partial \mathbf{v}'}\cdot\left[\left(1 - \frac{\mathbf{k}\cdot\mathbf{v}'}{\omega}\right)\mathbf{I} + \frac{\mathbf{k}\mathbf{v}'}{\omega}\right]\cdot\hat{\mathbf{E}}\right\}. \tag{24}$$

Equations (16), (20), and (21) with ϵ, ϵ_R, and ϵ_L defined by (17), (22), and (23) now combine to produce the form of Eq. (14). The only task remaining is to evaluate f_ϕ^{NL} and f_-^{NL} according to (18) and (24). This is a straightforward if tedious routine and is outlined in the Appendix; we simply state below the expressions for the coupling coefficients:

$$C_R = -\frac{i}{4}\frac{\omega_p^2}{V_e^2}\sum_{n=-\infty}^{+\infty}\frac{\omega_0}{\sqrt{2}k_\parallel V_e}\left(\frac{(Z - Z_R)\{\lambda_n(1 - n[(n-1)/\beta] + n\Omega/\omega_0\} + \lambda_n'(1 - n + 2\beta + \beta\Omega/\omega_0)\}}{\omega_0 + \Omega - n\Omega} + \frac{\omega_-\beta\lambda_n'(Z_1 - Z) + \beta\lambda_n'[\sqrt{2}k_\parallel V_e + (\omega - n\Omega)Z]}{\omega_-(\omega_0 - n\Omega)} + \frac{[n\lambda_n' - (n^2/\beta)\lambda_n + 3\beta\lambda_n'][\sqrt{2}k_\parallel V_e + (\omega - n\Omega - \Omega)Z_1]}{\omega_-(\omega_0 - n\Omega)}\right), \tag{25}$$

$$B_R = +\frac{i}{2}\frac{\omega_-}{c^2}\frac{\omega_p^2}{V_e^2}\sum_{n=-\infty}^{+\infty}\frac{1}{\sqrt{2}k_\parallel V_e}\left(\frac{[(n\Omega - \omega_0)\lambda_n + \beta\Omega\lambda_n'][\omega(Z - Z_R) + (\omega_0 - n\Omega + \Omega)Z_R]}{\omega_0 + \Omega - n\Omega} + \frac{\beta\Omega\omega_0\lambda_n' Z_R + \omega_0[n\lambda_n' - (n^2/\beta)\lambda_n + 2\beta\lambda_n'][\sqrt{2}k_\parallel V_e + (\omega_- - \Omega)Z_R]}{\omega_0 - n\Omega}\right). \tag{26}$$

As discussed in the Appendix, the symmetry in the problem is such that $C_L(\Omega) = C_R(-\Omega)$ and $B_L(\Omega) = B_R(-\Omega)$ so that it is unnecessary to express C_L and B_L explicitly. In (25) and (26) the following definitions apply: $Z = Z(\omega - n\Omega/\sqrt{2}k_\parallel V_e)$, $Z_R = Z(\omega_- - \Omega/\sqrt{2}k_\parallel V_e)$, $Z_1 = Z(\omega - n\Omega - \Omega/\sqrt{2}k_\parallel V_e)$, $\lambda_n = I_n(\beta)\exp -\beta$, and $\lambda_n' = (\partial/\partial\beta)[I_n(\beta)\exp -\beta]$. The coupling coefficients simplify considerably in the limit that Landau damping becomes weak; generally the Bernstein waves are the only ones to experience any significant damping.

Having derived expressions for the coupling terms we turn next to a discussion of the results obtained by solving Eq. (14) numerically.

III. DISCUSSION

Equation (14) has been solved numerically to determine the real and imaginary parts of the complex frequency ω as a function of the parallel wavenumber component, $k_\parallel$, of the scattered waves. Results are shown in Figs. 1–6 as plots of the growth rate γ of each Bernstein wave against $k_\parallel$ for a variety of densities and magnetic field strengths. In the figures the harmonic index n indicates Bernstein waves with frequencies lying within the range $n\Omega < \omega < (n+1)\Omega$. The numbers on the curves, at various positions in $k_\parallel$ space, give the frequencies of the waves and are normalized to ω_0. The essential physics becomes transparent on inspection of the form of Eq. (14).

When the magnetic field is small both the terms within the parentheses of (14) contribute equally to the growth of the instability; this is simply because the right and left circularly polarized waves are indistinguishable when $\Omega \to 0$. For larger fields, however, the two waves become sufficiently distinct such that we can regard the decay into right and left circularly polarized waves as being separate. In this parameter range one term within the parentheses generally dominates and an approximate expression for the growth rate may be derived from (14), valid in the fluid limit[15]:

$$\gamma_{R,L} \sim \gamma_0(1 \pm 3\Omega/\omega_0)/\sqrt{2}. \tag{27}$$

This expression is accurate provided $\gamma_0 \gg \Omega\omega_p^2/(\omega_p^2 + k_\parallel^2)$, where γ_0 is the field-free growth rate.

From Eq. (27) it is easily seen that the growth rate of the left circularly polarized wave decreases with increasing magnetic field strength. The growth rate of the right circularly polarized wave can be greater than the field-free growth rate γ_0 provided $1 + 3\Omega/\omega_0 > \sqrt{2}$. We expect to observe similar behavior from the kinetic model and, in addition, structure on the two oppositely polarized scattered light waves caused by the excitation of electron Bernstein waves.

A brief recap of the behavior of electrostatic waves in magnetized plasmas will aid interpretation of the results. For propagation parallel to the magnetic field the usual Bohm–Gross dispersion relation is obtained, modified by the presence of Landau damping. For perpendicular propagation the familiar Bernstein waves emerge propagating in between harmonics of the electron-cyclotron frequency. In oblique propagation, the nature of the waves is determined by the relative magnitudes of $k_\perp$ and $k_\parallel$. Thus, for small values of $k_\parallel$ we expect to see well separated (in frequency space) Bernstein modes, whereas as when $k_\parallel$ increases we would expect to observe the Bernstein modes merge to frequencies lying on or near the Bohm–Gross dispersion curve; we search for such behavior in the results.

Figure 1 shows the growth rates of Bernstein waves which can be excited at a density corresponding to $\omega_p/\omega_0 = 0.36$ and an electron temperature such that $V_e/c = 0.1$ (in all cases v_0, the electron quiver velocity, is set equal to $0.1c$). When $\Omega/\omega_0 = 0.01$ the growth curve is essentially the field-free result for which $\gamma/\omega_0 \sim 0.02$. For $\Omega/\omega_0 = 0.2$, on the other hand, waves in the bands $n\Omega < \omega < (n+1)\Omega$, $n = 1,2$ can be driven unstable. The large feature merging with the smaller one in the figure corresponds to right-hand circularly polarized waves (R); the two smaller ones to left-hand circularly polarized waves (L). Note that the latter have smaller growth rates than the main feature of the R branch and thus the growth rates have broadly similar behavior to that predicted by (27), which was derived in the fluid limit. For $k_\parallel = 0$ the branch of the Bernstein wave dispersion relation $2\Omega < \omega < 3\Omega$ contains the cold upper-hybrid frequency and thus the wave excited in this frequency interval is expected, in certain parameter ranges, to have behavior broadly similar to that predicted by a fluid treatment.

Moving to higher density (see Fig. 2) in which $\omega_p/\omega_0 = 0.42$, the R branch of the dispersion relation is located at a smaller value of $k_\parallel$ than that seen in Fig. 1 ($k_\parallel = 0$ corresponds to the reflection point of the scattered light waves). Only the $n = 2$ mode in the R wave appears since the $n = 1$ branch has a vanishingly small growth rate at this density. The L branch also moves to lower $k_\parallel$ but now growth of the $n = 2$ mode is larger than in Fig. 1. Note that the separation of the two peaks in the L branch increases in going from Fig. 1 to Fig. 2, i.e., in moving to smaller values of $k_\parallel$. Thus, as we move to higher densities, and hence to smaller $k_\parallel$, the discrete nature of the Bernstein waves begins to manifest itself. This is further seen in Fig. 3, where the $n = 1$ and $n = 2$ modes excited in the L wave are well separated at a higher density corresponding to $\omega_p/\omega_0 = 0.48$. At this density the R wave is absent since its reflection point occurs at lower density, i.e., at $\omega_p/\omega_0 = 0.41$ as shown in Fig. 2. The solid line in Fig. 3 is for $\Omega/\omega_0 = 0.01$ and again is

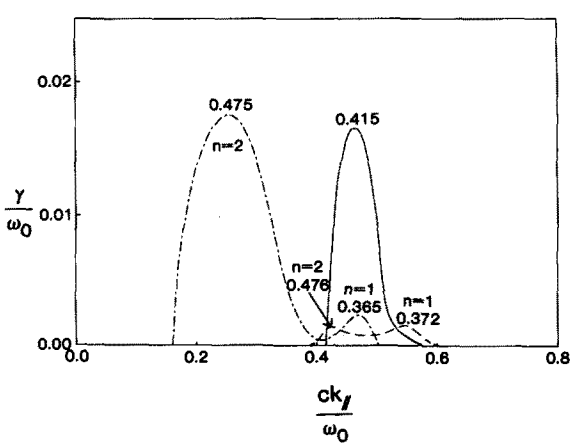

FIG. 1. Growth rates as functions of k for (a) R waves $\Omega/\omega_0 = 0.2$ (hatched line), (b) L waves $\Omega/\omega_0 = 0.2$ (long dashed line), (c) $\Omega/\omega_0 = 0.01$ (solid line), $\omega_p/\omega_0 = 0.36$.

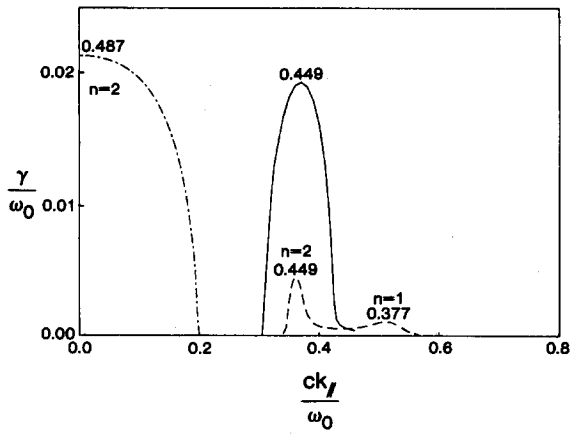

FIG. 2. Growth rates as functions of k for (a) R waves $\Omega/\omega_0 = 0.2$ (hatched line), (b) L waves $\Omega/\omega_0 = 0.2$ (long dashed line), (c) $\Omega/\omega_0 = 0.02$ (solid line), $\omega_p/\omega_0 = 0.41$.

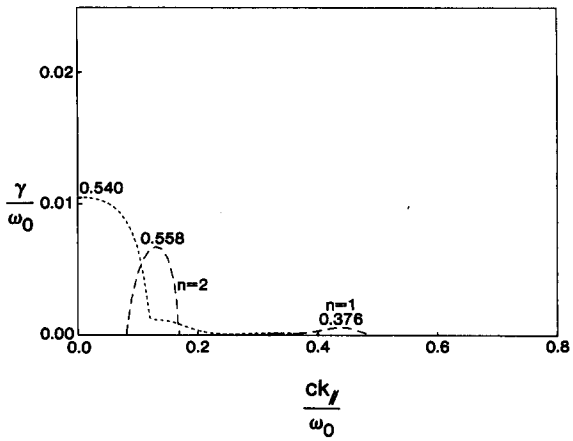

FIG. 4. Growth rates as functions of k for L waves $\Omega/\omega_0 = 0.1$ (short dashed line), $\Omega - \omega_0 = 0.2$ (long dashed line), $\omega_p/\omega_0 = 0.51$.

identical with the field-free growth rate. This wave is almost at its reflection point at this particular density.

Consider now a still higher density, at which $\omega_p/\omega_0 = 0.51$, i.e., beyond the quarter-critical density, as shown in Fig. 4. Only L waves can be driven unstable at this density and choice of magnetic field, i.e., $\Omega/\omega_0 = 0.1, 0.2$. When $\Omega/\omega_0 = 0.2$, the $n = 1$ and $n = 2$ modes are well separated for the reasons discussed above. Note that the effect of the magnetic field is to extend growth of the L waves to densities greater than quarter-critical. Thus at $\Omega/\omega_0 = 0.1$ the main feature in the L wave is near its reflection point, whereas at $\Omega/\omega_0 = 0.2$ the mirror point is at a higher density corresponding to $\omega_p/\omega_0 \sim 0.53$. The growth rate in the case $\Omega/\omega_0 = 0.1$ differs little from that predicted by (27), except that it has a tail which is modulated at frequencies corresponding to excitation of lower order Bernstein waves; these waves have $\gamma/\omega_0 < 10^{-4}$ and are consequently of no significance.

Figure 5 illustrates results obtained for a parameter choice such that $\omega_p/\omega_0 = 0.45$, $\Omega/\omega_0 = 0.01$, 0.10, and 0.20. The R branch is again absent at this density when $\Omega/\omega_0 = 0.2$, whereas when $\Omega/\omega_0 = 0.10$ it is beginning to emerge. By comparing Fig. 5 with Fig. 2 it can be seen that growth of the main branch of the R wave is larger at $\Omega/\omega_0 = 0.2$ than at $\Omega/\omega_0 = 0.1$. This behavior is again essentially that predicted by Eq. (27) so there is little difference between the two descriptions for these parameters.

For the R waves the most interesting parameter range occurs when Ω/ω_0 is of the order of 0.15–0.17 as illustrated in Fig. 6. Under these circumstances the R branch separates into two features with almost equal growth rates. These correspond to the excitation of $n = 2$, 3 Bernstein waves as the frequencies shown would indicate. The L branch broadens in $k_\parallel$ space to encompass the $n = 1$–3 harmonic frequency range but no distinct structure emerges. As the R wave separates in $k_\parallel$ space with increasing magnetic field, the growth rate decreases below that predicted by (27) and thus significant departures from the results of fluid theory can arise in this parameter range.

IV. CONCLUSIONS

The effects of a dc magnetic field on stimulated Raman sidescattering have been studied using a kinetic model. The scattered light waves are in the form of right and left circularly polarized waves with a frequency separation proportional to the magnitude of the field. The growth rates of the left circularly polarized waves decrease with increasing mag-

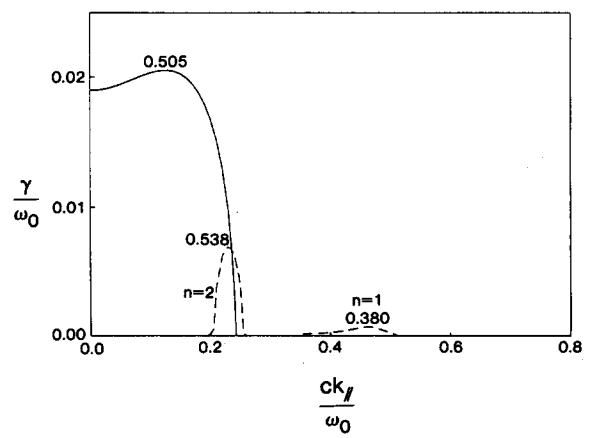

FIG. 3. Growth rates as functions of k for (a) L waves $\Omega/\omega_0 = 0.2$ (long dashed line), (b) $\Omega/\omega_0 = 0.01$ (solid line), $\omega_p/\omega_0 = 0.48$.

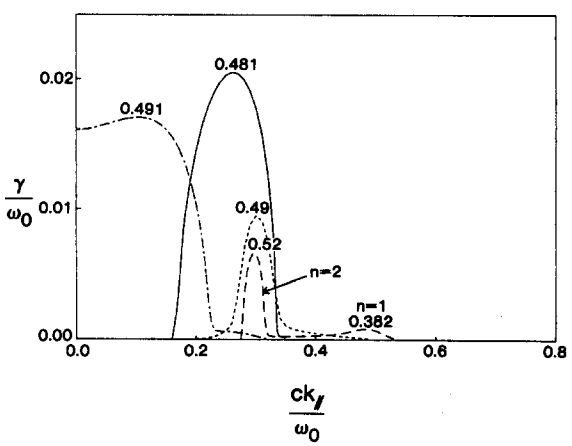

FIG. 5. Growth rates as functions of k for (a) R waves $\Omega/\omega_0 = 0.1$ (hatched line), (b) L waves $\Omega/\omega_0 = 0.1$ (short dashed line), $\Omega/\omega_0 = 0.2$ (long dashed line), $\omega_p/\omega_0 = 0.45$.

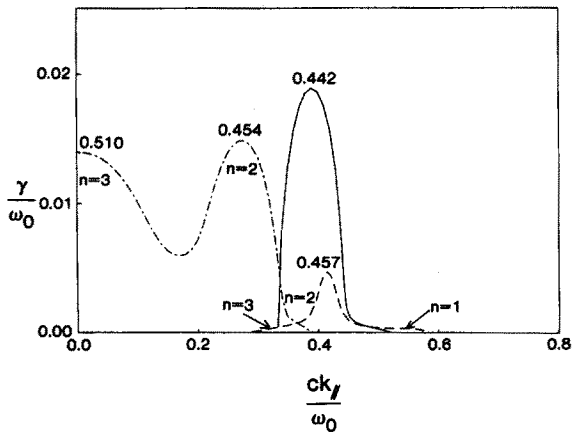

FIG. 6. Growth rates as functions of k for (a) R waves $\Omega/\omega_0 = 0.16$ (hatched line), (b) L waves $\Omega/\omega_0 = 0.16$ (long dashed line), (c) $\Omega/\omega_0 = 0.01$, $\omega_p/\omega_0 = 0.40$.

netic field, and for sufficiently strong fields, structure is induced in the frequency spectrum as a result of coupling to electron Bernstein waves. For $\Omega/\omega_0 < 0.1$, no additional structure appears in either the R or the L wave; the field only results in a broadening of the frequency spectrum. The right-hand circularly polarized wave has enhanced growth in certain parameter ranges, e.g., at $\Omega/\omega_0 = 0.2$ and $\omega_p/\omega_0 = 0.4$. At intermediate field values, notably at $\Omega/\omega_0 = 0.15$, the R wave has two components with almost equal growth rates; the growth rates are also lower than those predicted by fluid theory. The fields required to induce these modes in experiments using one micron light are larger than any so far observed. For small magnetic fields the results differ very little from our earlier work. This theory offers a possible explanation of results from recent experiments on $\omega_0/2$ emission, but because of the large fields required it is doubtful that it would be the dominant effect.

APPENDIX: INTEGRATION OF COUPLING COEFFICIENTS

To evaluate the integrals in Eqs. (7), (18), and (24), we use the unperturbed electron trajectories determined by

$$\frac{d\mathbf{v}}{dt} = \mathbf{v}\times\boldsymbol{\Omega}, \quad \frac{d\mathbf{r}}{dt} = \mathbf{v}.$$

These equations are solved routinely for $\mathbf{r}$ and $\mathbf{v}$ in cylindrical coordinates. In the text the differential operator $\partial/\partial\mathbf{v}$ is given by

$$\frac{\partial}{\partial\mathbf{v}} = \hat{\mathbf{x}}\cos\theta\frac{\partial}{\partial v_\perp} + \hat{\mathbf{y}}\sin\theta\frac{\partial}{\partial v_\perp} + \hat{\mathbf{z}}\frac{\partial}{\partial v_\parallel} + \frac{1}{v_\perp}(\hat{\mathbf{y}}\cos\theta - \hat{\mathbf{x}}\sin\theta)\frac{\partial}{\partial\theta}.$$

With the set of quantities $\{\mathbf{r},\mathbf{v},\mathbf{r}',\mathbf{v}'(\partial/\partial\mathbf{v}),(\partial/\partial\mathbf{v}')\}$ evaluated, and the linear distribution functions given by (8)–(11), f_ϕ^{NL} and f_-^{NL} can be computed straightforwardly from (18) and (24). To obtain the coupling coefficients B and C of Eq. (14), the expressions for f_ϕ^{NL} and f_-^{NL} are substituted into the right-hand sides of Eqs. (16), (20), and (21). Notice that the integral over $\mathbf{v}$ in these expressions is of the form

$$\int_0^{2\pi} d\theta \int_{-\infty}^{+\infty} dv_\parallel \int_0^{\infty} v_\perp \,(\text{expression})\, dv_\perp.$$

The integral over θ presents no problem and the coupling terms then appear as integrals over the two remaining variables $v_\perp$ and $v_\parallel$, i.e.,

$$\begin{aligned}
C_R = {} & \frac{i}{2}\pi\omega_p^2\frac{eE_{0y}}{m}\sum_{n=-\infty}^{+\infty}\int_{-\infty}^{+\infty}dv_\parallel\int_0^{\infty}dv_\perp \\
& \times\left\{\left[4v_\perp^3\frac{\partial}{\partial v_\perp^2}\left(\frac{\partial f_0^0}{\partial v_\perp^2}\right)\left(J_nJ_n'' + \frac{n\Omega}{k_0v_\perp}J_nJ_n'\right) - 2v_\perp J_n^2\frac{\partial f_0^0}{\partial v_\perp^2} + 2\frac{k_0v_\perp^2}{\omega_0}J_nJ_{n-1}\frac{\partial f_0^0}{\partial v_\perp^2}\right]\right. \\
& \times[(\omega_- - k_\parallel v_\parallel - \Omega)(\omega - k_\parallel v_\parallel - n\Omega)]^{-1} \\
& + \left[\frac{k_\parallel v_\perp^2}{\omega_-}\frac{\partial}{\partial v_\parallel}\left(\frac{\partial f_0^0}{\partial v_\perp}\right)\left(\frac{n\Omega}{k_0v_\perp}J_nJ_n' - J_n'^2\right) - \left(1 - \frac{k_\parallel v_\parallel}{\omega_-}\right)\frac{k_0v_\perp}{\Omega}\frac{\partial f_0^0}{\partial v_\perp}J_nJ_n'\right]\{(\omega_0 - n\Omega)(\omega - k_\parallel v_\parallel - [n+1]\Omega)\}^{-1} \\
& \left.+ \left[\left(1 - \frac{k_\parallel v_\parallel}{\omega_-}\right)\frac{k_0v_\perp}{\Omega}\frac{\partial f_0^0}{\partial v_\perp}J_nJ_n'\right][(\omega_0 - n\Omega)(\omega - k_\parallel v_\parallel - n\Omega)]^{-1}\right\}. \qquad \text{(A1)}
\end{aligned}$$

Having found C_R no further effort is required to obtain C_L since inspection of Eq. (14) shows that a symmetry between the various coefficients must exist. This is most easily seen when considering what happens when $\Omega \to 0$, for which it is obvious that $C_R \to C_L$; with a finite magnetic field the symmetry is such that $C_R(-\Omega) = C_L(\Omega)$. A similar symmetry exists for B_R and B_L, i.e., $B_R(-\Omega) = B_L(\Omega)$ with B_R defined by

$$\begin{aligned}
B_R = {} & i\pi\omega_p^2\frac{eE_{0y}^*}{m}\sum_{n=-\infty}^{+\infty}\int_{-\infty}^{+\infty}dv_\parallel\int_0^{\infty}dv_\perp \\
& \times\left\{\left[k_0v_\perp\left(\frac{\partial f_0^0}{\partial v_\perp}\right)J_nJ_n' - k_\parallel v_\perp^2\frac{\partial}{\partial v_\parallel}\left(\frac{\partial f_0^0}{\partial v_\perp}\right)J_n'J_{n+1}\right][(\omega_0 - n\Omega)(\omega_- - k_\parallel v_\parallel - \Omega)]^{-1}\right. \\
& \left.+ \frac{\partial f_0^0}{\partial v_\perp}\left(\frac{\omega}{\omega - k_\parallel v_\parallel - n\Omega} - 1\right)\left(\frac{J_n^2 - (k_0v_\perp/\omega_0)J_nJ_{n-1}}{\omega_- - k_\parallel v_\parallel - \Omega}\right)\right\}. \qquad \text{(A2)}
\end{aligned}$$

On defining the plasma dispersion function as

$$Z(\eta)=\frac{1}{\pi^{1/2}}\int_{-\infty}^{+\infty}\frac{e^{-x^2}\,dx}{x-\eta}, \tag{A3}$$

making use of the integral formulas

$$\int_0^\infty v_\perp J_n^2 e^{-v_\perp^2/2V_e^2}\,dv_\perp = V_e^2 I_n(\beta)e^{-\beta}, \tag{A4}$$

$$\int_0^\infty v_\perp^2 J_n J_n' e^{-v_\perp^2/2V_e^2}\,dv_\perp = \frac{V_e^4 k_0}{\Omega}\frac{\partial}{\partial\beta}(I_n(\beta)e^{-\beta}), \tag{A5}$$

$$\int_0^\infty v_\perp^3 [J_n']^2 e^{-v_\perp^2/2V_e^2}\,dv_\perp = V_e^4\left(\frac{n^2}{\beta}-2\beta\frac{\partial}{\partial\beta}\right)I_n(\beta)e^{-\beta}, \tag{A6}$$

and using standard recurrence relations between the Bessel functions, the coupling coefficients can be expressed in the form given by Eqs. (25) and (26) in Sec. II of the text.

[1]M. N. Rosenbluth, Phys. Rev. Lett. **29**, 565 (1972).
[2]D. W. Forslund, J. M. Kindel, and E. L. Lindman, Phys. Rev. Lett. **30**, 739 (1973); Phys. Fluids **18**, 1002, 1017 (1975).
[3]C. S. Liu, M. N. Rosenbluth, and R. B. White, Phys. Fluids **17**, 1211 (1974).
[4]J. F. Drake, P. K. Kaw, Y. C. Lee, G. Schmidt, C. S. Liu, and M. N. Rosenbluth, Phys. Fluids **17**, 778 (1974).
[5]K. G. Estabrook, W. L. Kruer, and B. F. Lasinski, Phys. Rev. Lett. **45**, 1399 (1980).
[6]W. L. Kruer, K. Estabrook, B. F. Lasinski, and A. B. Landon, Phys. Fluids **23**, 1326 (1980).
[7]C. Joshi, T. Tajima, J. M. Dawson, H. A. Baldis, and N. A. Ebrahim, Phys. Rev. Lett. **47**, 1285 (1981).
[8]D. W. Phillion, E. M. Campbell, K. G. Estabrook, G. E. Phillips, and F. Ze, Phys. Rev. Lett. **49**, 2405 (1982).
[9]A. A. Offenberger, R. Fedosejevs, W. Tighe, and W. Rozmus, Phys. Rev. Lett. **49**, 371 (1982).
[10]K. Tanaka, L. M. Goldman, W. Seka, M. C. Richardson, J. Soures, and E. A. Williams, Phys. Rev. Lett. **48**, 1179 (1982).
[11]D. W. Phillion, D. L. Banner, E. M. Campbell, and R. E. Turner, Phys. Fluids **25**, 1434 (1982).
[12]S. M. L. Sim and E. McGoldrick, Opt. Commun. **40**, 433 (1982).
[13]R. E. Turner, D. W. Phillion, B. F. Lasinski, and E. M. Campbell, Phys. Fluids **27**, 511 (1984).
[14]T. Tajima and J. M. Dawson, Phys. Rev. Lett. **43**, 267 (1979).
[15]H. C. Barr, R. Rankin and T. J. M. Boyd, Phys. Lett. A **105**, 218 (1984); H. C. Barr, T. J. M. Boyd, L. R. T. Gardner, and R. Rankin, Phys. Fluids **27**, 2730 (1984).
[16]J. A. Stamper, E. A. McLean, and B. H. Ripin, Phys. Rev. Lett. **40**, 1177 (1978).
[17]A. Raven, O. Willi, and P. T. Rumsby, Phys. Lett. A **71**, 435 (1979).
[18]A. Raven, P. T. Rumsby, J. A. Stamper, O. Willi, R. Illingworth, and R. Thareja, Appl. Phys. Lett. **35**, 526 (1979).
[19]T. J. M. Boyd, D. Cooke, and G. J. Humphreys-Jones, Phys. Lett. A **88**, 140 (1982).
[20]O. Willi, P. T. Rumsby, and C. Duncan, Opt. Commun. **37**, 40 (1981).
[21]C. E. Max, *Laser Plasma Interactions*, edited by R. Balian and J. C. Adam (North-Holland, Amsterdam, 1982), p. 301.
[22]C. Joshi, C. E. Clayton, and F. F. Chen, Phys. Rev. Lett. **48**, 874 (1982).
[23]O. Willi, P. T. Rumsby, C. Hooker, A. Raven, and Z. Q. Lin, Opt. Commun. **41**, 110 (1982).
[24]O. Willi, P. T. Rumsby, and S. Sartang, IEEE J. Quant. Elect. **QE-17**, 1909 (1981).